# CAVITATION INCEPTION ON SHIP PROPELLER MODELS

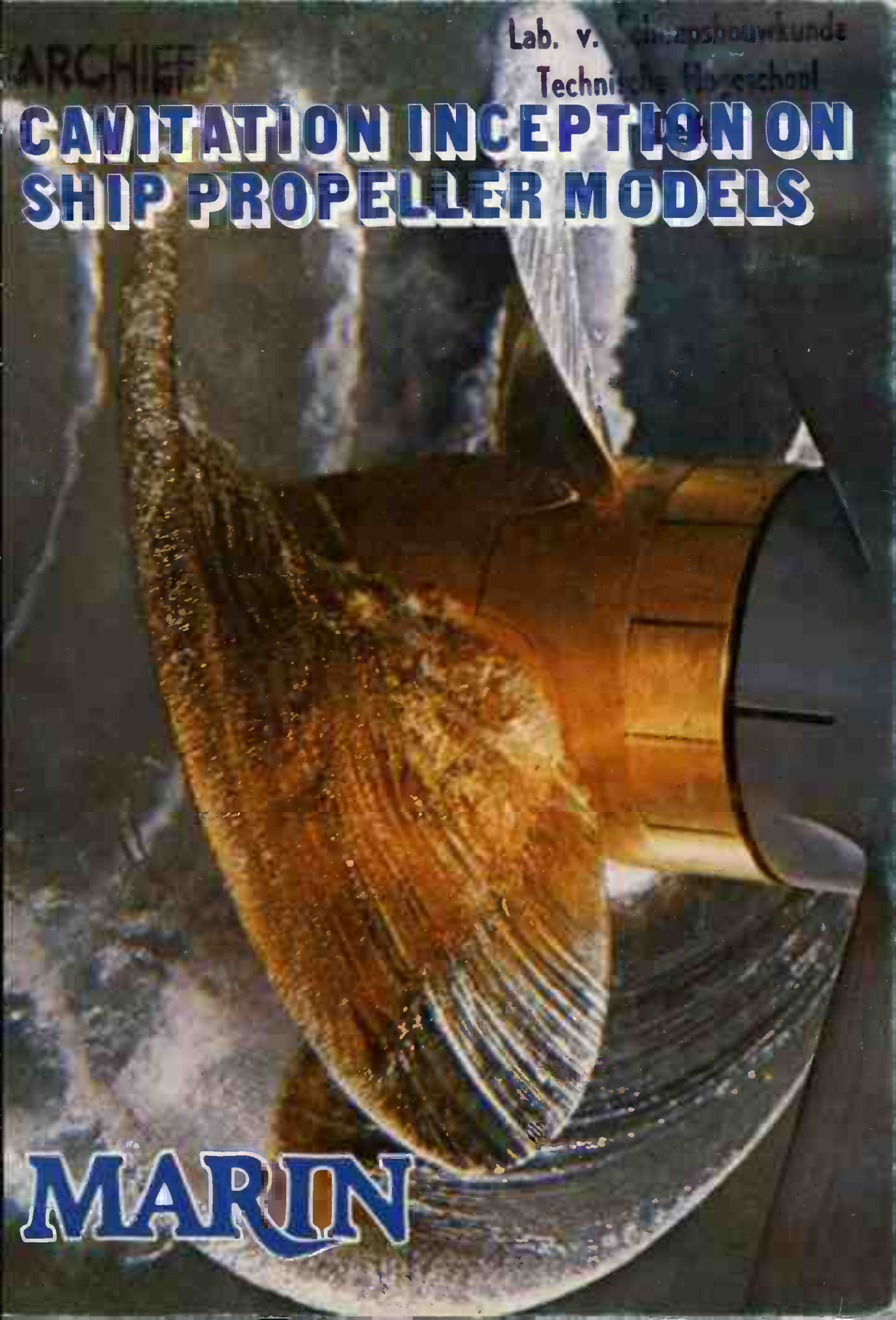

MARIN

# CAVITATION INCEPTION ON SHIP PROPELLER MODELS

Dr. G. KUIPER

Publication No. 699 of the Netherlands Ship Model Basin – The Wageningen-Ede Laboratories of MARIN – 1983.

This publication is a summary of the full report with the same title, published as NSMB publication No. 655.

Cover and Photography:
Th. W. Boekhorst,
MARIN Audio Visual Department.

MARIN

# MARITIME RESEARCH INSTITUTE NETHERLANDS
# NSMB, WAGENINGEN/EDE LABORATORIES OF MARIN

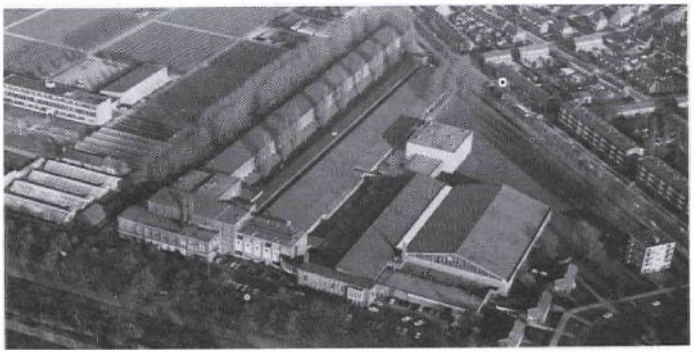

Aerial view of the NSNB Laboratories in Wageningen

Wageningen Laboratories: Haagsteeg 2
P.O. Box 28, 6700 AA Wageningen
The Netherlands – Telephone +31 8370 93911
Cables: Modeltank – Telex: 45148 nsmb nl

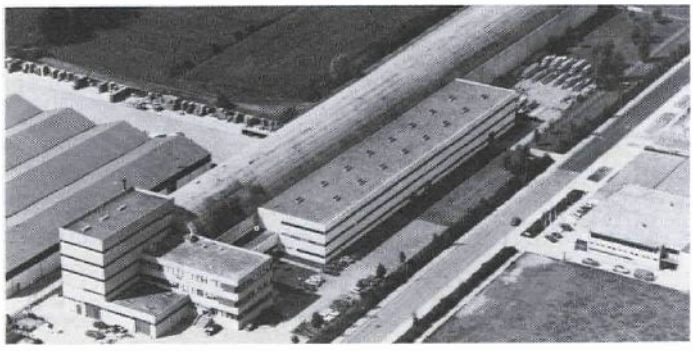

Aerial view of the De-pressurized Towing Tank situated in Ede

Ede Laboratory: Niels Bohrstraat 10
6716 AM Ede – The Netherlands
Telephone +31 8380 37177

Rotterdam office: Keizerstraat 9
P.O. Box 1555, 3000 BN Rotterdam – The Netherlands
Telephone +31 10 114768 – Telex: 27067 nemar nl

# Marin

The Maritime Research Institute Netherlands (MARIN) in Wageningen/Ede and Rotterdam is an independent foundation working on a non-profit basis. The object of MARIN is to perform scientific research in hydrodynamics, economics, navigation and sociology, affording an integral approach in solving the present-day maritime problems.

MARIN has originated from the merger of the Netherlands Ship Model Basin (NSMB) in Wageningen/Ede and the Netherlands Maritime Institute (NMI) in Rotterdam.

NSMB was founded in 1929 by the Dutch Government and four large shipping companies. Work started in Wageningen in 1932. In the early days, the industrial orders mainly related to optimization of hull forms and propulsion devices by means of model tests in a deep-water basin.

In its endeavours to provide a highly scientific level of industrial service, NSMB has continuously explored new fields of specialized service to the shipbuilding, shipping and offshore industries. The character of these specialized services implies that they are often not carried out within industries themselves.

As a consequence of this philosophy, development of special-purpose laboratories has gradually taken place, resulting in the building of cavitation tunnels, the seakeeping basin, the shallow water basin, the high-speed towing tank, the wave and current basin, the depressurized towing tank and the ship-manoeuvring simulators.

NMI was founded in the early seventies to cover specific areas of maritime research which until then had remained unexplored, notably navigation research and maritime social research. Moreover, the need was felt to integrate several smaller facilities to create an organized entity with a proper balance between the necessary maritime disciplines.

NMI was given the task of carrying out economic research, navigation research, operations research and planning, and social research.

At present (1983) MARIN's staff consists of about 420 persons, of whom 140 have a higher professional education. The annual turnover of scientific industrial orders roughly amounts to 45 million Dutch guilders (19 million U.S. dollars) of which approximately 60% comes from abroad. The activities of MARIN can be broadly subdivided as follows:

### Economic Research

- market forecasting
- optimization of transport systems
- feasibility studies
- ports and terminals consultancy

### Ship powering

- hull optimization

- propeller design
- cavitation

**Ocean Engineering**
- seakeeping
- fixed and floating structures
- mooring systems

**Navigation Research and Ship Handling**
- design of traffic separation schemes
- transport risk and analyses
- marine accident analysis
- transport safety research
- manoeuvring tests
- simulation studies
- nautical aspects of harbours and fairways
- training

**Management and Organization Development**
- consultancy services
- post graduate courses

**Computer Services**
- preliminary ship design calculations
- programmes for shipyard production

## NSMB testing facilities

| *Name of facility* | *Dimensions in metres* | *Type of tests* |
|---|---|---|
| 1. Deep-water basin | 252 × 10.5 × 5.5 | Resistance, propulsion, vibratory forces, etc. |
| 2a. Large cavitation tunnel | 0.9 × 0.9 (test section) | Cavitation tests with propellers, profiles etc. in various types of flows, fluctuating pressures on hull. |
| 2b. Cavitation tunnel with flow regulator | 0.4 circular test section | Cavitation tests with propellers in simulated axial wake. |
| 2c. High speed cavitation tunnel | 0.04 circular test section | Fundamental cavitation studies. |
| 3. Computer centre CDC Cyber 175 computer, 2 paper tape drawing machines | | Hydrostatic, stability, trim, etc. calculations. Design of ships, including economic calculations. |
| 4. Seakeeping laboratory | 100 × 24.5 × 2.5 (pit depth 6) | Ship motion measurements; necessary power increase to maintain speed; bottom and deck pressures; water shipment and screw racing, wave-induced shear forces, bending and torsional moments; measurements on semi-submersibles etc. All in regular and irregular waves. |
| 5. Shallow water basin | 216 × 15.75 × 1.25 (water-depth is variable) | Resistance and propulsion in shallow water; squat and trim measurements; transverse forces, yawing moment and rudder torque on captive model; resistance and performance in waves; ship motions in regular and irregular waves; motions, mooring and anchor-line forces of semi-submersibles or moored structures; oscillation tests; manoeuvring tests, etc. |
| 6. Wave and current laboratory | 60 × 40 × 1.20 (water-depth is variable) (pit depth 3) | Determination of feasibility of vessel configurations, with respect to waves, current and wind; motion and force measurements; spiral and turning circle tests; tests on mooring systems, etc. |
| 7. High speed towing tank | 220 × 4 × 4 | Testing planing hulls; high speed propulsion devices; ice breaking studies in simulated ice fields; testing offshore structures in waves. |
| 8. Manoeuvring simulator (hybrid computer) | | Training in ship handling, development of navigational aids; design of harbour entrances; development of criteria for manoeuvring, etc. |
| 9. Depressurized towing tank | 240 × 18 × 8 | Resistance, propulsion and propeller cavitation tests; flow visualization tests; wave breaking phenomena at the bow; wake surveys; propeller-induced vibratory forces in shaft and on hull; acoustical measurements; etc. |

CONTENTS

# 1. Introduction

## 1.1. CAVITATION

Cavitation in a fluid occurs when the pressure is low, usually in regions with a high flow velocity. Due to the low pressure, parts of the fluid can become vapor. The regions in which vapor exists are called cavities. Cavitation inception occurs when the process of vaporisation begins.

## 1.2. CAVITATION INCEPTION

Vapor and fluid are in equilibrium when the pressure in the cavity is at the vapor pressure. In practical cases the pressure in a cavity is indeed close to the vapor pressure. However, to obtain inception a much lower pressure in the fluid is often necessary. In that case there is a threshold for cavitation. This threshold can be very high. Briggs (Journal of Appl. Phys., 1950) found cavitation inception in pure standing water only at a pressure of -277 bars, while the equilibium pressure was at +12.5 mbar !

Usually water is not very pure and contains solid particles as well as air. This makes the threshold lower, but also unpredictable.

## 1.3. SCALING OF CAVITATION

Cavitation on ship propellers is investigated on model scale in a cavitation tunnel or in a depressurized towing tank, where the size of the ship propeller is reduced with the scale factor $\lambda$. To obtain a similar condition as on the prototype two scaling parameters have to be maintained, viz. the advance ratio J and the cavitation index $\sigma_n$, where

$$J = \frac{U}{nD} \qquad (1)$$

$$\sigma_n = \frac{p_o - p_v}{\frac{1}{2}\rho n^2 D^2} \qquad (2)$$

The advance ratio J is a measure for the propeller loading and can be replaced by the thrust coefficient $K_T$, where

$$K_T = \frac{T}{\rho n^2 D^4} \qquad (3)$$

| | | | |
|---|---|---|---|
| where: | T | = propeller thrust | N |
| | U | = advance velocity of the propeller | $m\ sec^{-1}$ |
| | n | = rotation rate of the propeller | $sec^{-1}$ |
| | D | = propeller diameter | m |
| | $p_o$ | = static pressure at the shaft | $Nm^{-2}$ |
| | $\rho$ | = specific mass of water | $kg\ m^{-3}$ |
| | $p_v$ | = vapor pressure | $Nm^{-2}$ |

The influence of gravity and of the presence of a free water surface above the propeller will be ignored in this publication. The propeller inflow on model- and full scale are assumed to be similar in every respect.

## 1.4. CAVITATION SCALE EFFECTS

When both the advance ratio (and thus the propeller loading) and the cavitation index are the same on the model and the prototype the cavitation pattern on the model propeller is also similar to that on the prototype, provided that inception also takes place at the vapor pressure.

As mentioned, this is not always the case and this leads to differences between the cavitation on the model and on the prototype. These differences are called scale effects on cavitation inception.

There are other possible scale effects, e.g. on the propeller inflow. These effects will not be addressed in this report.

## 1.5. NUCLEI

The bond between the water molecules, which prevents inception of cavitation, can be broken by the presence of small amounts of free gas. Due to the surface tension this gas will be present in the form of small spherical bubbles with a diameter of say 10 to 100 μm. These bubbles are called nuclei.

In sea water these nuclei are constantly generated by breaking waves and probably also by micro organisms. In a cavitation tunnel these bubbles are generated by the pump or are recirculating from the cavitating test body. In standing water, as in a depressurized towing tank, these bubbles will either dissolve due to the surface tension or will rise to the surface. Free gas may still be present in standing water, e.g. in cracks of small solid particles.

Consider the growth of two nuclei of 20 and 100 μm initial diameter when the pressure decreases linearly to zero. Assuming that no gas dissipation occurs through the bubble wall the result is shown in Figure 1. There is a distinct point at which the bubble growth becomes very rapid. This is the pressure at which the gas bubble becomes unstable and this pressure is called the critical pressure $p_c$

$$p_c = p_v - \frac{4s}{3R_{crit}} \tag{4}$$

in which $R_{crit}$ is the radius of the gas bubble at the critical pressure

$$R_{crit} = (\frac{3}{2}\frac{K}{s})^{\frac{1}{2}} \tag{5}$$

s is the surface tension and K is a constant, depending on the amount of gas in the bubble, which depends on the initial conditions, e.g. on the initial bubble size $R_o$.

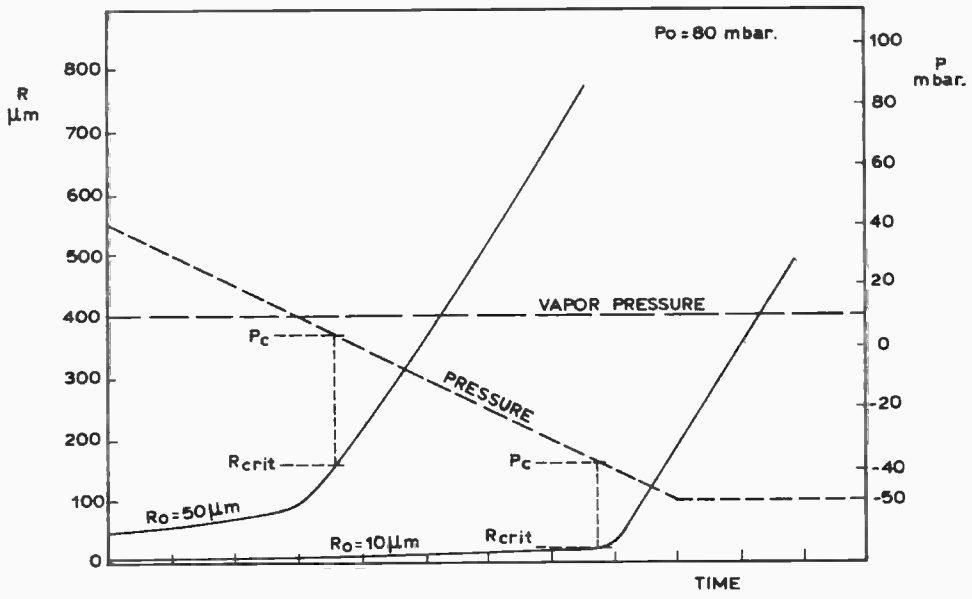


*Fig. 1. Bubble growth of air bubbles in water when the pressure decreases.*

Since the bubble growth is very rapid when the pressure is below the critical pressure we can consider the critical pressure as the inception pressure. From eqs. 4 and 5 two important features of the thus defined inception pressure can be found:

- the inception pressure is always lower than the vapor pressure,
- the inception pressure depends on the amount of gas in the nucleus, so on its initial size.

## 1.6. VISCOUS EFFECTS

From investigations on headforms (e.g. Arakeri and Acosta, Journal of Fluids Eng., 1973) it is known that also the boundary layer on a body can affect the inception pressure, especially the transition of the

boundary layer from laminar to turbulent flow or the existence of a separation bubble. A separation bubble occurs when the laminar boundary layer separates from the wall. This separated shear layer is unstable, becomes turbulent and reattaches to the wall. Thus a short "dead-water region" is formed below the boundary layer, the so-called laminar separation bubble.

These viscous effects influence cavitation inception probably by local low pressures occurring in the transition region or in the reattachment region. The critical pressure, as described in section 1.5, is no longer the mean pressure on the body or on the propeller blade, but is the minimum pressure occurring in the boundary layer. Apart from the nuclei size distribution the inception pressure consequently also becomes dependent on the boundary layer, which is controlled by the Reynolds number and by the pressure distribution on the blades. (The blades are considered smooth and the influence of turbulence on the boundary layer will be ignored in this publication)
The Reynolds number on the propeller blades can be characterized by the propeller Reynolds number

$$Re_n = \frac{nD^2}{\nu} \qquad (6)$$

Since on the prototype of a propeller blade the boundary layer will be turbulent in the minimum pressure point (where inception occurs), the aim will be to attain a turbulent boundary layer at that point on model scale as well.

## 1.7. PURPOSE OF THIS PUBLICATION

At the Netherlands Ship Model Basin the influence of the nuclei content of the fluid and of the boundary layer of the propeller blades on cavitation inception on model propellers was investigated. Also some means to reduce the scale effects of the experiments were developed. The results were published in a thesis (Kuiper, NSMB Public. No. 655, 1981). In the present publication these results are summarized and discussed

with special emphasis on practical application in cavitation tests and in cavitation prediction.

The Plates at the end of this publication are from the thesis. They are referred to when useful in this report. A short description pertaining to the Plates is given in the Appendix.

# 2. Experimental investigations

## 2.1. THE EXPERIMENTAL APPROACH

Experiments were carried out with propeller models in uniform axial inflow. This made it possible to investigate inception of cavitation on propeller blades without creating a complex interaction between the propeller inflow and the propeller itself. Scale effects on propeller inflow are thereby excluded.

## 2.2. TYPES OF CAVITATION

The pressure distribution on propeller blades determines the type of cavitation. When a sharp low-pressure peak exists at the leading edge of the propeller blades sheet cavitation will occur. When the pressure drop is gradual and the minimum pressure occurs away from the edges bubble cavitation will occur. In the tip region of the propeller blades a vortex can be generated, depending on the loading of the propeller tips, which leads to tip vortex cavitation.

Since the inception conditions can be different for these types of cavitation three propellers were designed, exhibiting these three types of cavitation exclusively in design condition. Propeller S has thin blades with little camber, which leads to sheet cavitation. Propeller B has thick blades and larger camber, leading to bubble cavitation. Both propellers S and B have a strongly reduced pitch at the tip to avoid tip vortex cavitation. Propeller V has nearly the same pitch at all radii, leading to a strong tip vortex. The geometry of these propellers is given in Figure 2.

The mentioned types of cavitation are typical on ship propellers. Other types, as cavitation in free shear layers, were not investigated because on ship propellers separated flow regions are generally avoided.

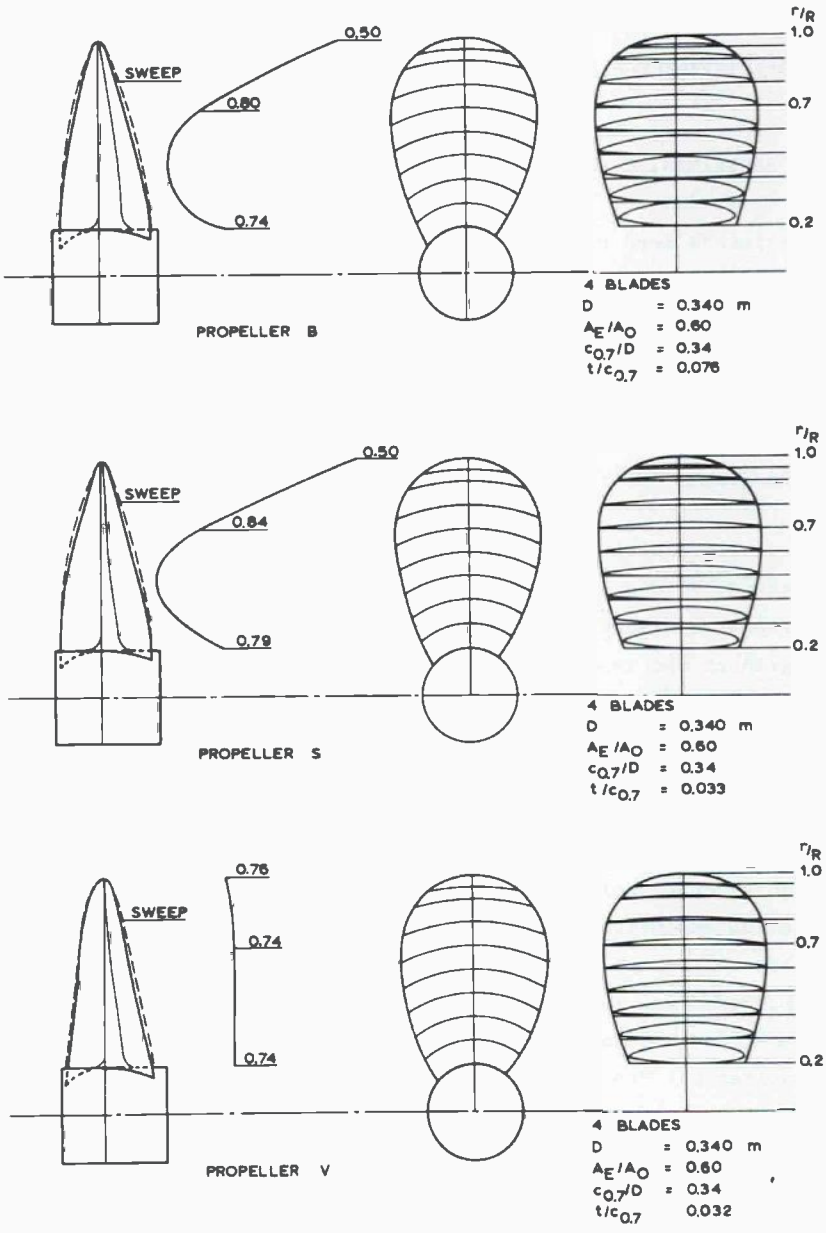


*Fig. 2. Geometry of Propellers.*

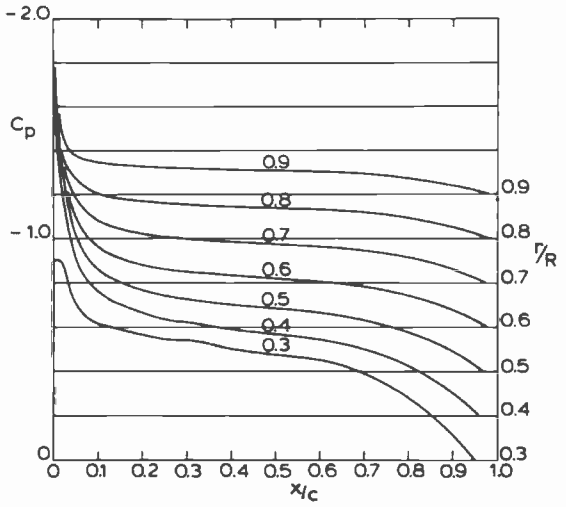


*a. J = 0.4.*

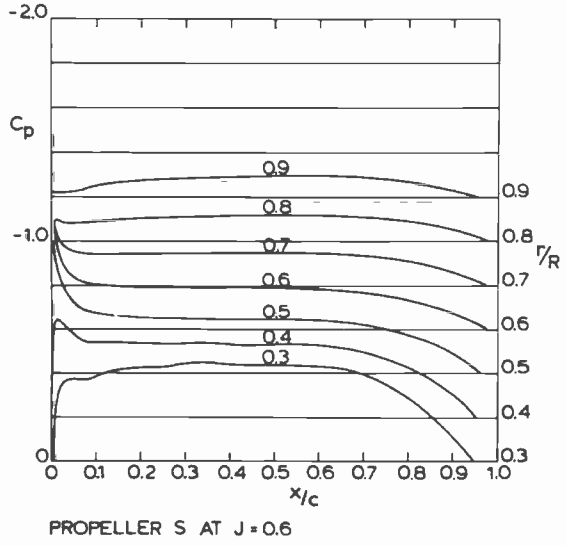


*b. J = 0.6.*

*Fig. 3a.b. Pressure distribution on the suction side of propeller S.*

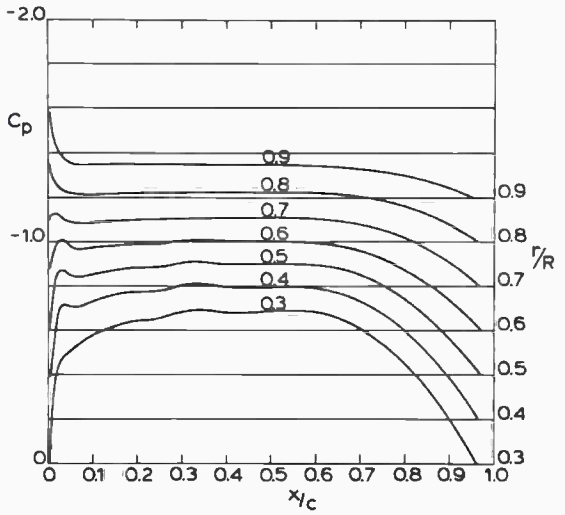


*c. J = 0.4.*

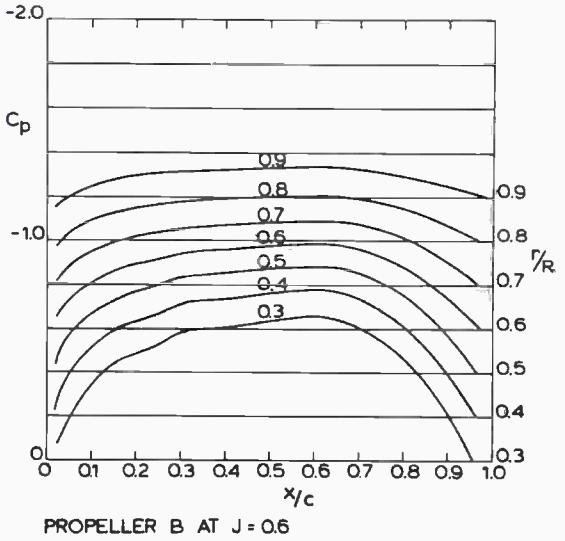


*d. J = 0.6.*

*Fig. 3c.d. Pressure distribution on the suction side of propeller B.*

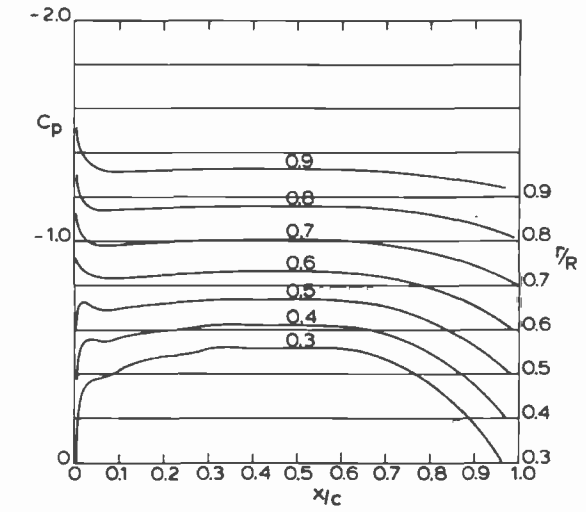


*e. J = 0.4.*

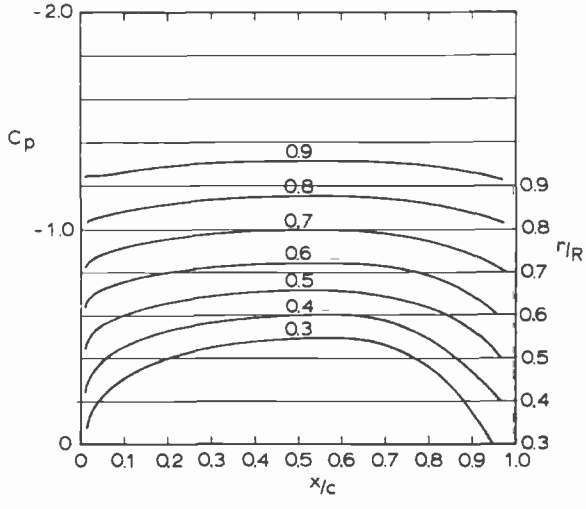


*f. J = 0.6.*

*Fig. 3e.f. Pressure distribution on the suction side of propeller V.*

The choice of uniform axial inflow also means that the cavitation pattern on the propellers is nearly steady and independent of the blade position. Cloud cavitation, occurring behind unsteady sheet cavitation, is therefore also not investigated. This type of cavitation, however, is typical for developed cavitation and does not pose inception problems.

## 2.3. THE CALCULATED PRESSURE DISTRIBUTION ON PROPELLERS B, S AND V

The pressure distribution on the suction side of the propellers B, S and V, is given in Figures 3a to f. Note that in these figures the basis of the pressure coefficient at each radius is shifted as indicated at the right hand side. The indicated $C_p$ scale refers to r/R = 0.3 and should be shifted for other radii too.

These pressure distributions are given for two different propeller loadings. The pressure distribution is given in dimensionless form as the sectional pressure coefficient $C_p$. The vapor pressure generally is made non-dimensional in a similar way as the sectional cavitation index $\sigma$. (For definitions see the list of nomenclature). When no cavitation scale effects occur inception of cavitation will take place at a certain propeller section when

$$\sigma = - C_{p(min)} \qquad (7)$$

When cavitation on propeller blades is assessed both the sectional cavitation index $\sigma$ and the minimum pressure coefficient have to be compared as a function of the radius. (Note that the sectional cavitation index is different from the propeller cavitation index $\sigma_n$, as given in eq. 2).

## 2.4. THE TEST FACILITIES

The tests were carried out in two facilities:
the NSMB large cavitation tunnel and the NSMB Depressurized Towing Tank. An impression of both facilities is given in Figures 4 and 5.

The conditions in both facilities are different (nuclei content, Reynolds number) and comparison of the results from both facilities is important to assess the scale effects in each facility.

## 2.5. STIMULATION OF INCEPTION

Since cavitation inception is always delayed as compared with the theoretical criterion of eq. 7, some inception stimulating measures were developed in order to reduce the scale effects.

Electrolysis was applied to generate bubbles upstream of the propeller. An electric tension between two poles results in the formation of hydrogen and oxygen out of water. In the towing tank the poles were sets of thin

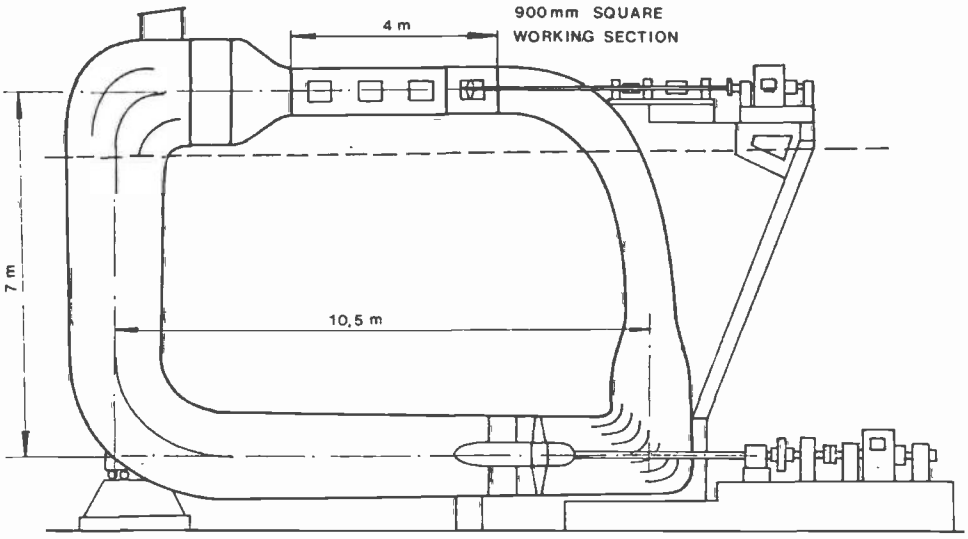


*Fig. 4. The NSMB Large Cavitation Tunnel.*

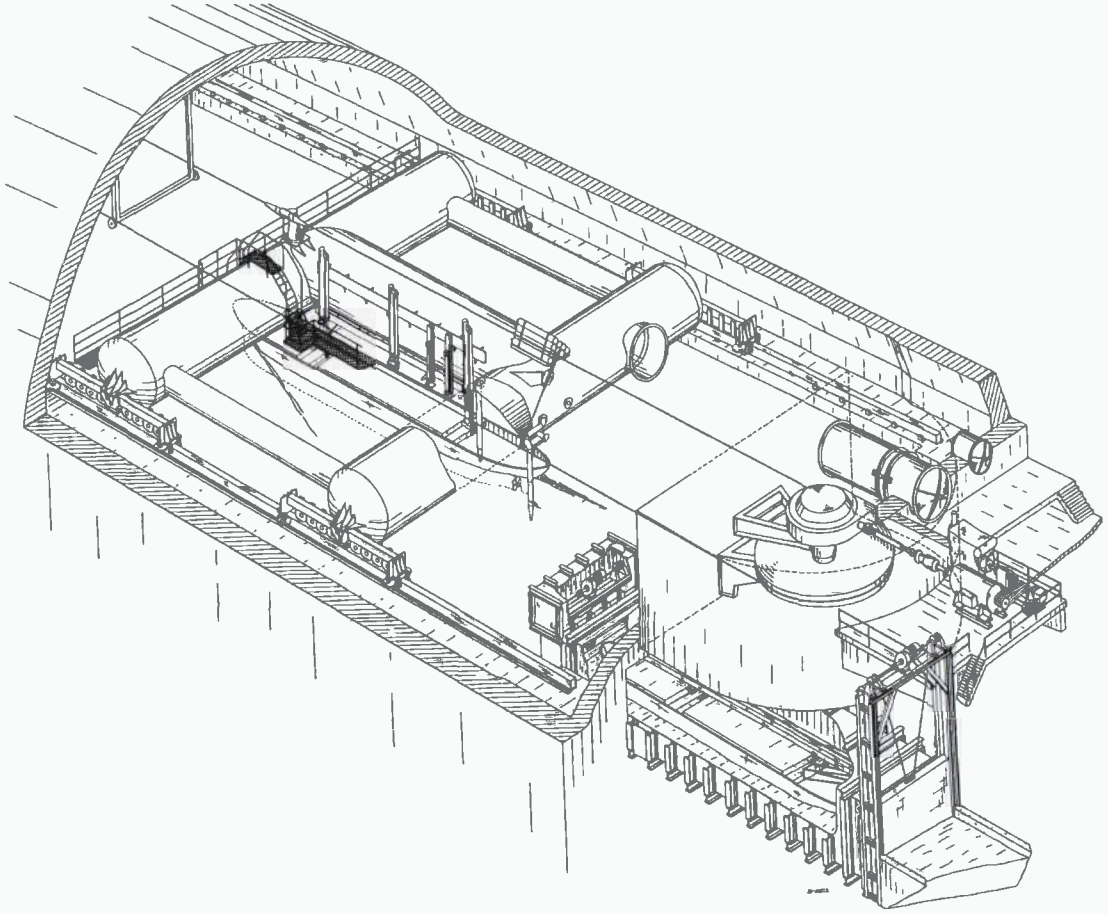

*Fig. 5. The NSMB Depressurized Towing Tank.*

wires (0.3 mm in diameter), in the cavitation tunnel the poles were thin steel strips, glued to a wooden foil. In both cases these devices were mounted 1.6 m upstream of the propeller. Variation of the voltage between the poles varies the electric current and thus the amount of gas produced.

Artificial roughness was applied at the leading edge of the blades (over about 1 mm) to change the boundary layer. The roughness elements were 60 µm carborundum particles, glued to the surface with a very thin layer of laquer. The roughness was applied over a very short distance only, so that the own resistance of the roughness elements was negligible and the propeller performance was not affected significantly.

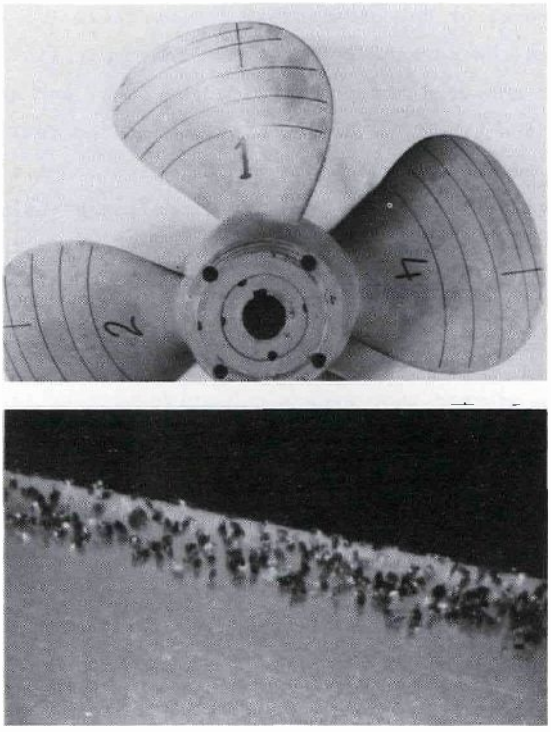


*Fig. 6. Application of roughness at the leading edge.*

# 3. The boundary layer on the blades of propeller models

The boundary layer on a foil starts at the stagnation point as a laminar boundary layer. In the transition region, the location of which depends among others on the Reynolds number, this laminar boundary layer changes into a turbulent one. Because the friction coefficient of a turbulent boundary layer is much higher than that of a laminar one, the position of the transition to turbulence influences the drag of the foil. In terms of propeller forces this means that the propeller torque (and to a lesser degree also the propeller thrust) depends on the location of transition.

When the propeller Reynolds number is increased (by increasing the rotation rate and the advance velocity simultaneously) the transition region will move upstream towards the leading edge and the torque will increase. Since the propeller Reynolds number of the full scale propeller is very high it can be expected that in that case transition occurs very close to the leading edge. Therefore the propeller Reynolds number of the model propeller has to be high enough to have the transition region near the leading edge too, so that regions of laminar boundary layer flow are avoided.

It is often assumed that such a condition without laminar boundary layer flow is obtained when the propeller torque becomes nearly independent of the Reynolds number. Based on measurements of propeller thrust and torque as a function of Reynolds number a minimum sectional Reynolds number of $2 \times 10^5$ at 0.7 R is often chosen as a criterion for turbulent boundary layer flow on the model propeller. This corresponds with a propeller Reynolds number of about $1.5 \times 10^5$ for the propellers under investigation.

Since it is assumed that above this Reynolds number transition occurs close to the leading edge no scale effects on cavitation inception were expected.

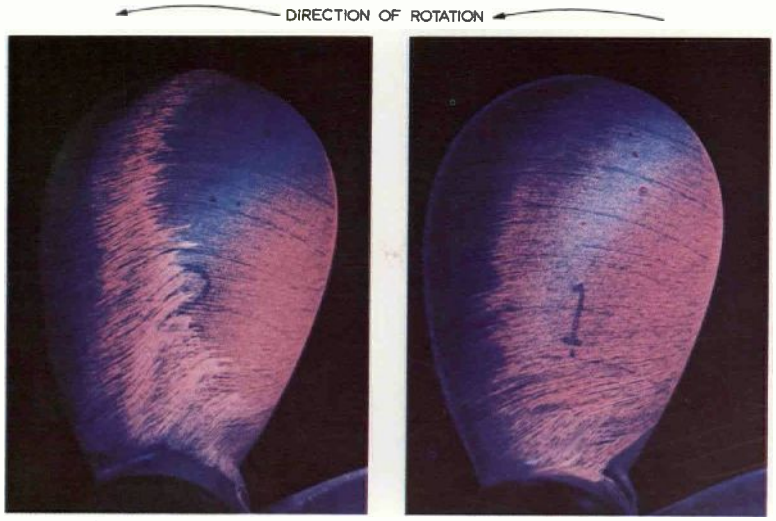


*PLATE 3.1. EXAMPLE OF PAINT TEST WITH AND WITHOUT ROUGHNESS AT THE LEADING EDGE. PROPELLER B AT J=0,4, $Re_n$=1.7x10$^6$.*

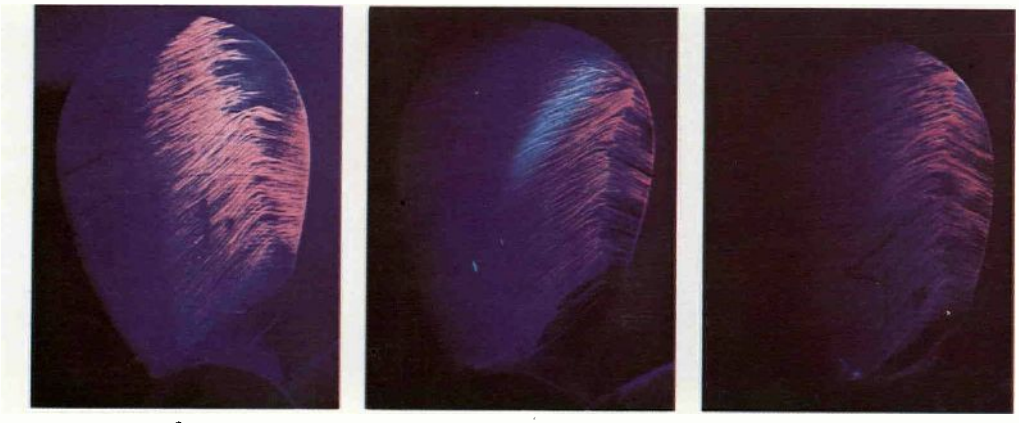


*PLATE 3.4. PAINT PATTERNS ON THREE PROPELLERS WITH DIFFERENT SIZE (J=0.6, $Re_n$=1.1x10$^6$).*

$Re_n = 1.1 \times 10^6$

$Re_n = 1.7 \times 10^6$

*PLATE 3.10. PAINT PATTERN ON PROPELLER B AT J=0,6.*

$Re_n = 1.1 \times 10^6$

$Re_n = 1.7 \times 10^6$

*PLATE 3.11. PAINT PATTERN ON PROPELLER B AT J=0.4.*

$Re_n = 1.1 \times 10^6$ $Re_n = 1.7 \times 10^6$

*PLATE 3.14. PAINT PATTERN ON PROPELLER S AT J=0.6.*

*PLATE 3.15. PAINT PATTERN ON PROPELLER S AT J=0.4. $Re_n = 1.1 \times 10^6$.*

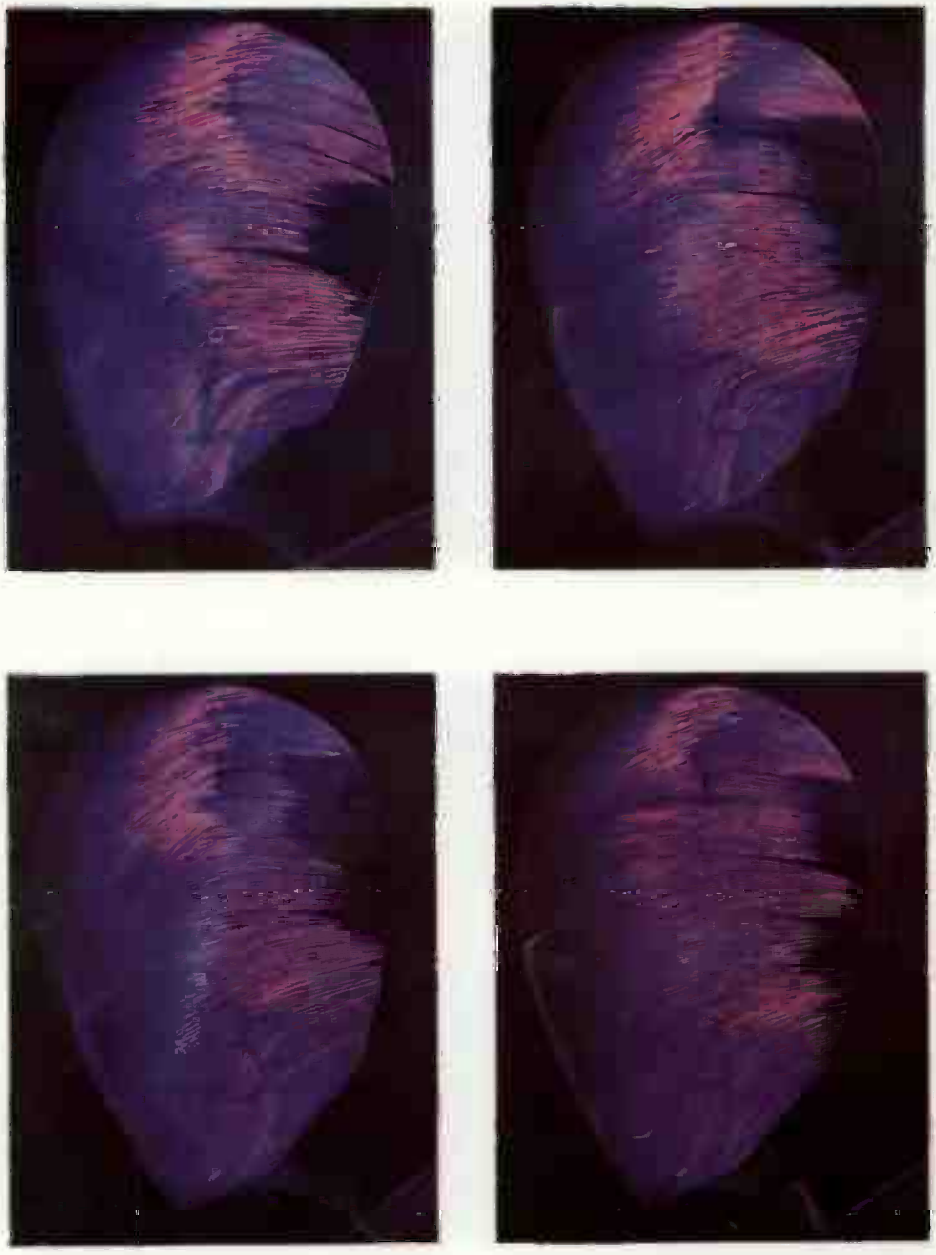

*PLATE 3.17. DIFFERENCES BETWEEN THE BLADES WHEN LAMINAR SEPARATION OCCURS.* IV
*(PROPELLER S AT J=0.55, $Re_n$=1.1x10$^6$ ).*

J = 0.60

J = 0.55

J = 0.50

J = 0.45

J = 0.40

*PLATE 3.18. THE PAINT PATTERN ON PROPELLER S AT VARIOUS LOADINGS.* V
*($Re_n$=1.1x10$^6$).*

$Re_n = 1.1 \times 10^6$

PLATE 3.13. PAINT PATTERN ON PROPELLER B* AT J=0.85.

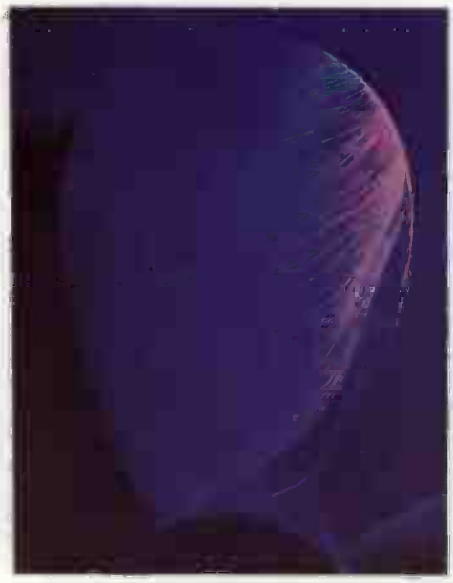

$Re_n = 0.56 \times 10^6$

PLATE 3.12. PAINT PATTERN ON PROPELLER B* AT J=0.28.

$Re_n = 1.1 \times 10^6$

$Re_n = 1.7 \times 10^6$

PLATE 3.20. PAINT PATTERN OF PROPELLER V AT J=0.4.

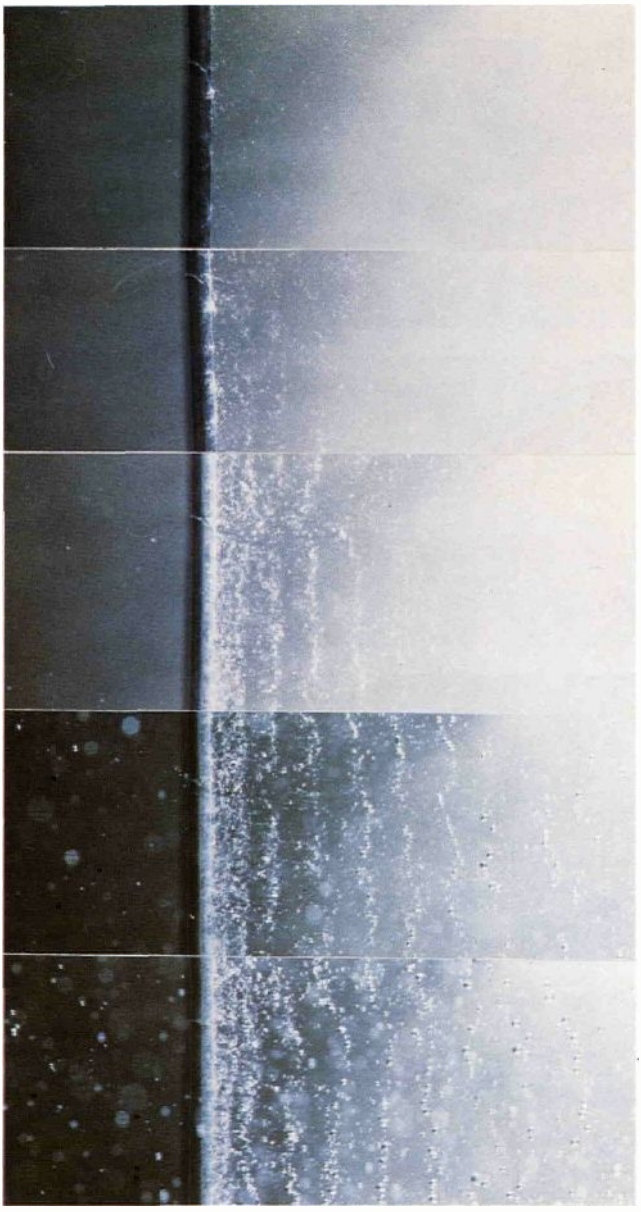


*PLATE 5.4. THE EFFECT OF GAS PRODUCTION ON ELECTROLYSIS.*
*(V=3 m/sec, p=270 mbar, WIRE DIAMETER 0.9 mm).*

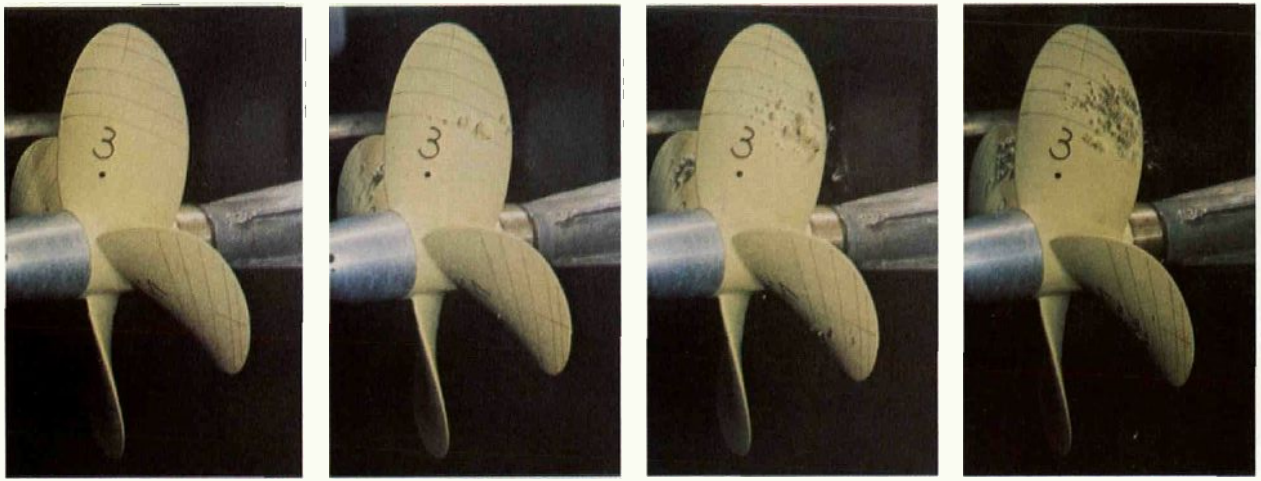

0 A/m 0.4 A/m 0.8 A/m 2.0 A/m

*PLATE 6.5. VARIATION OF ELECTROLYSIS CURRENT ON PROPELLER B AT J=0.6. ($Re_n$=1.1x10$^6$, $\sigma_n$=1.0).*

WITHOUT ELECTROLYSIS

WITH ELECTROLYSIS

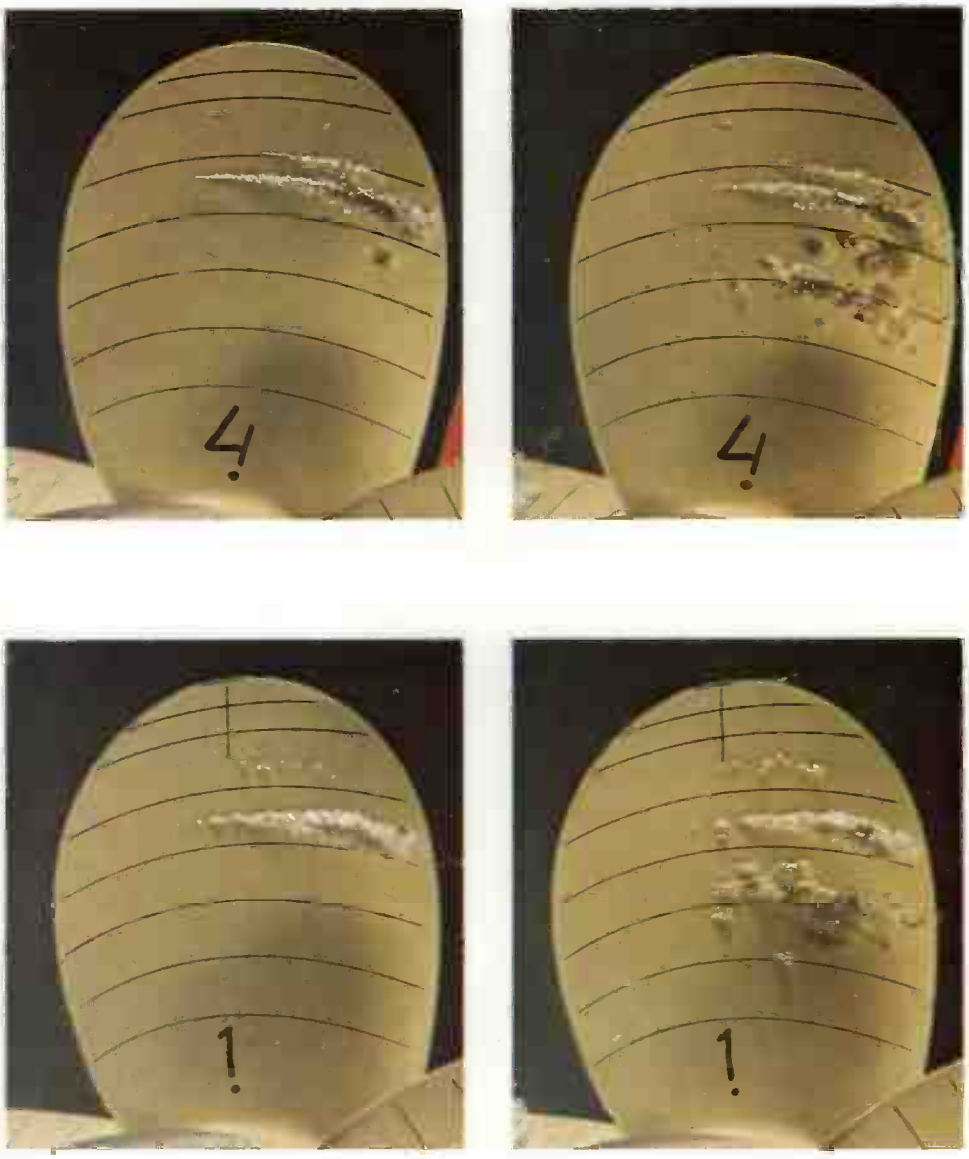


BLADE : 4 SMOOTH
BLADE : 1 ROUGHENED AT THE LEADING EDGE

*PLATE 6.6. CAVITATION OBSERVATIONS IN THE CAVITATION TUNNEL. PROPELLER B AT J=0.6. ($\sigma_n$=0.92, $Re_n$=2.11x10$^6$).*

WITHOUT ELECTROLYSIS

WITH ELECTROLYSIS

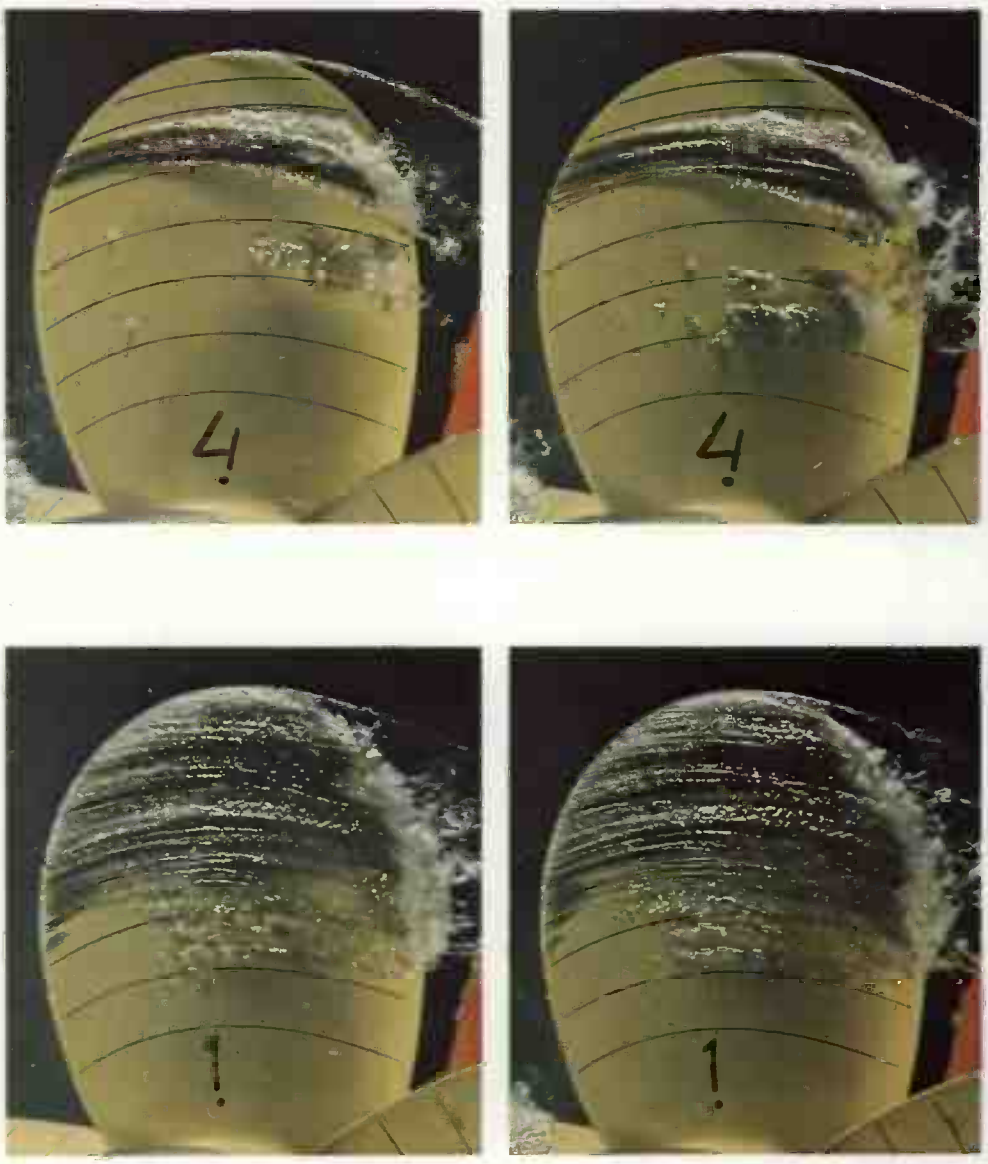


BLADE : 4 SMOOTH
BLADE : 1 ROUGHENED AT THE LEADING EDGE

*PLATE 6.10. CAVITATION OBSERVATIONS IN THE CAVITATION TUNNEL. PROPELLER B AT J=0.4. ($\sigma_n$=0.92, $Re_n$=2.11x10$^6$).*

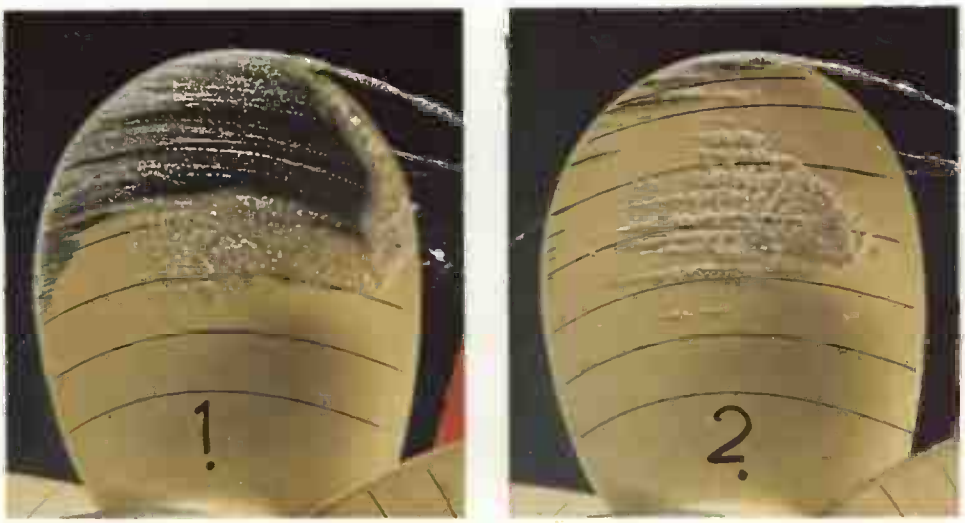


ROUGH SMOOTH

*PLATE 6.12. CAVITATION OBSERVATIONS IN THE CAVITATION TUNNEL AT HIGH REYNOLDS NUMBER. ($Re_n$=2.88x10$^6$, $\sigma_n$=1.15 ; J=0.4).*

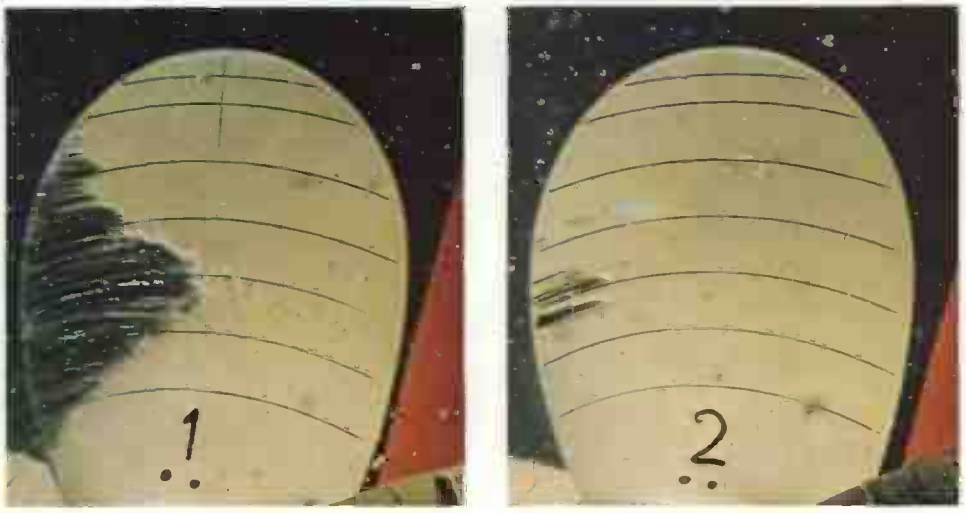


ROUGH SMOOTH

*PLATE 7.10. CAVITATION OBSERVATIONS IN THE CAVITATION TUNNEL ON PROPELLER S AT J=0.6. ($Re_n$=2.11x10$^6$, $\sigma_n$=0.92).*

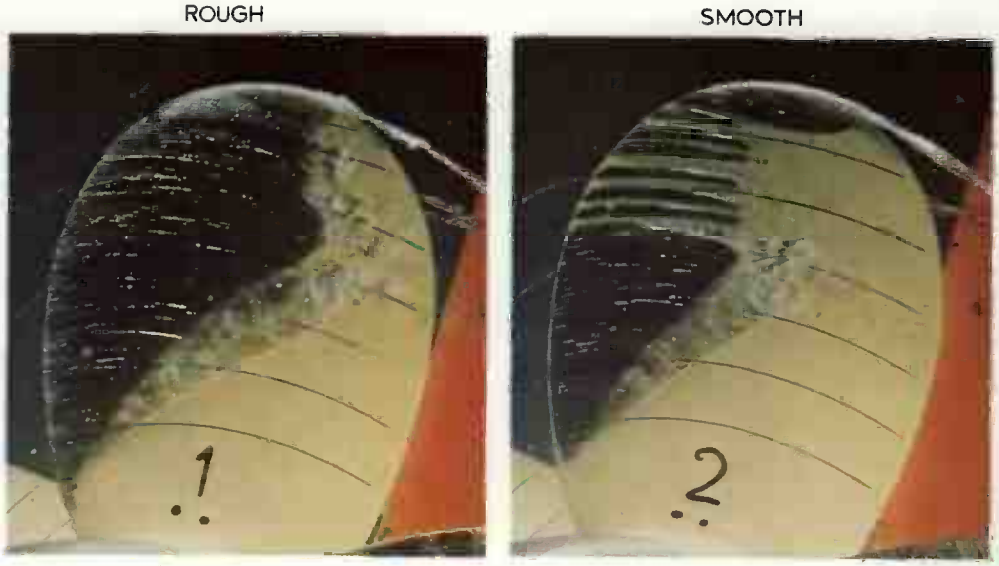


*PLATE 7.5. CAVITATION OBSERVATIONS IN THE CAVITATION TUNNEL ON PROPELLER S AT J=0.4. ($Re_n$=1.78x10$^6$, $\sigma_n$=1.3).*

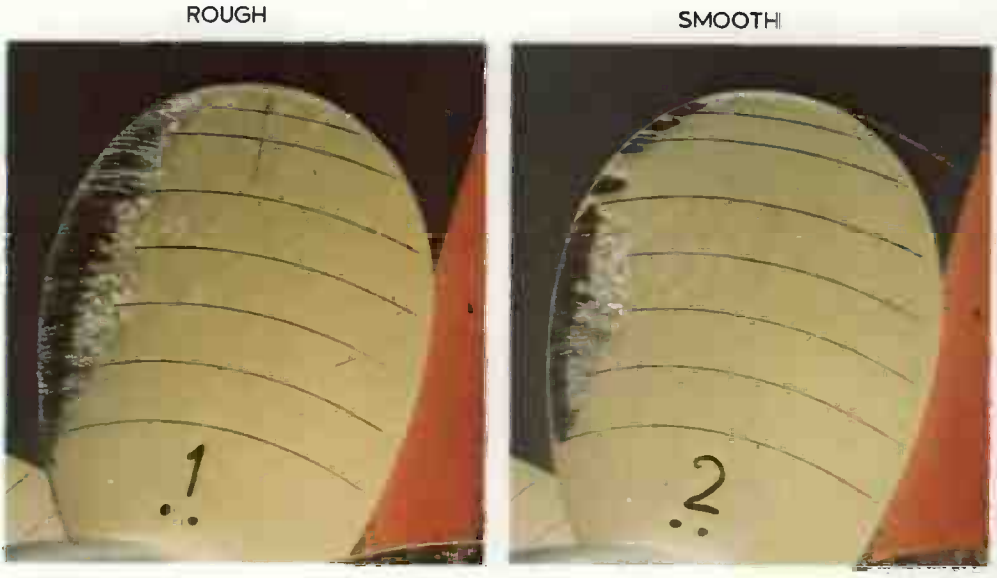


*PLATE 7.6. CAVITATION OBSERVATIONS IN THE CAVITATION TUNNEL ON PROPELLER S AT J=0.4. ($Re_n$=1.36x10$^6$, $\sigma_n$=2.2).*

Investigations with oil and paint on propeller blades reported in the literature (e.g. Meyne, 1972) indicated already that also in the case of a Reynolds independent thrust- and torque coefficient considerable regions with a laminar boundary layer could still exist on the blades. This would imply that the risk of boundary layer effects on cavitation inception remains. This will be investigated in the following sections.

## 3.1. PAINT TESTS

To investigate the boundary layer on propeller blades the paint test was further developed. In this paint test a layer of "paint" (lead-oxide with fluorescent pigment) was applied at the leading edge of the propeller, as shown in Figure 7.

The propeller was subsequently investigated at the required number of revolutions and forward speed, so that the paint formed very thin streaks on the propeller surface. These streaks were hardly visible by eye, but could be observed and photographed using ultra-violet illumination,

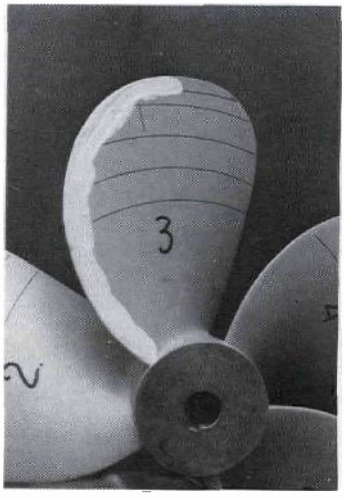


*Fig. 7. Application of paint.*

which made visible the fluorescent dye in the paint. The difference in friction between a laminar and a turbulent boundary layer causes a difference in thickness of the paint streaks. But, because the centrifugal force on the paint particles is constant at a certain radius, this difference in friction also causes a change in direction of the paint streaks. The streaks in a laminar boundary layer are more outwardly directed than those in a turbulent region.

This can be seen in Plate 3.1, where on the smooth blade the boundary layer on the suction side of propeller B is laminar until in the midst of the blade the streaks become thinner and change in direction, indicating transition from laminar to turbulent flow.

With these paint tests the effect of leading edge roughness can also be verified, as is shown in Plate 3.1. On the roughened blade the boundary layer is turbulent over nearly the whole blade area. Only near the hub some laminar regions remain.

## 3.2. RESULTS OF PAINT TESTS

The paint tests confirmed that considerable regions of laminar flow remained, both on the suction and on the pressure side of the blades. This is shown for the suction side of propeller B in Plates 3.1, 3.4, 3.10 and 3.11, for propeller S in Plate 3.14 and for propeller V in Plate 3.20. The lowest propeller Reynolds number used in these tests was $1.1 \times 10^6$, which is about four times higher than the criterion for Reynolds independent torque, as mentioned before.

These figures also show that an increase of the propeller Reynolds number has only a small effect on the position of transition. The propeller Reynolds number of $1.7 \times 10^6$ was the highest value which could be obtained in the Depressurized Towing Tank. Although higher Reynolds numbers are possible in a cavitation tunnel it is clear that this will generally be insufficient to bring the transition region close to the leading edge.

Transition occurs earlier in an adverse pressure gradient (when the pressure increases) and is delayed by a favourable pressure gradient. The pressure distribution on the propeller blade can therefore influence the location of transition. These effects, however, were also small on the propeller blades. Propeller S at J = 0.6 (Figure 3b) has a low pressure peak near the leading edge, very similar as propeller B at J = 0.4 (see Figure 3c). Still the transition region remains near midchord (Plates 3.11 and 3.14). This is also the case (Plate 3.10) when the pressure distribution near the leading edge is different, (Figure 3d) as on propeller B at J = 0.6.

The results of paint tests, as discussed until now, illustrate that it is very difficult indeed to move the transition region towards the leading edge. The fact that propeller thrust and torque are nearly Reynolds independent does not mean that no laminar boundary layer regions are present on the model propeller.

There are, however, two mechanisms which can create a turbulent boundary layer over the whole blade. These will be discussed next.

## 3.3. LAMINAR SEPARATION

When the pressure peak becomes very sharp the laminar boundary layer will separate from the blade surface and form a "separation bubble". This can be seen from the paint pattern of Plate 3.15. The occurrence of laminar separation is independent of the Reynolds number in the range of Reynolds numbers used on model propellers, and depends on the pressure distribution only. Laminar separation occurs abruptly when the pressure gradient increases, as is illustreated by the abrupt end of the separation bubble towards the blade tip. The chordwise length of the separation bubble can be very small, in the situation in Plate 3.15 the length is larger than usual. Downstream of the separation bubble the boundary layer is turbulent.

As will be shown later, laminar separation has a profound effect on cavitation inception. Therefore it is useful to point out the sensitivity of laminar separation to the pressure distribution, and thus to the shape of the leading edge.

Plate 3.15 illustrates that the laminar separation bubble extends more outward on blade 4 than on blade 2. Apparently this is caused by differences in blade geometry. This becomes even more pronounced at a somewhat lighter loading, as shown in Plate 3.17, where all blades are shown in the same condition. These differences could be traced to very small differences between the blades using a special blade edge microscope. So when laminar separation is about to occur the sensitivity for inaccuracies in the blade geometry increases dramatically.

The sensitivity of laminar separation to the pressure distribution also makes that a change in propeller loading changes the separation region rapidly. This is illustrated in Plate 3.18. At $J = 0.6$ the boundary layer is laminar and attached near the leading edge. The separated region grows rapidly with an increase in loading. The consequences of this sensitivity of laminar separation will be discussed later.

## 3.4. ROUGH SURFACE EFFECTS

Sometimes turbulent streaks were observed in regions of laminar flow, as on Plate 3.14 at the higher Reynolds number. This is caused by surface irregularities. Because the boundary layer becomes thinner with increasing Reynolds number the surface irregularities become relatively more important. At a certain Reynolds number these irregularities will trip the boundary layer to turbulence, specifically when they are in regions with an adverse pressure gradient, behind the minimum pressure point. When the Reynolds number is further increased these turbulent streaks will increase in number and make the boundary layer turbulent over the whole blade. This occurs frequently on propeller models. It must be emphasised that, although the boundary layer becomes turbulent from the leading edge, such a case

is different from the situation where natural transition takes place near the leading edge on a smooth blade. The latter condition would occur at a much higher Reynolds number, if the blades were completely smooth. When surface imperfections cause transition the blade is actually fully "roughened", although the roughness is due to insufficient finishing of the blades. This effect of inadvertent roughening is aggravated in a cavitation tunnel, where tiny particles, circulating with the tunnel water, attach themselves to the leading edge of the propeller model.

## 3.5. SOME FEATURES OF THE BOUNDARY LAYER ON NORMAL PROPELLER BLADES

The pitch near the tip of the blades of propellers B and S is strongly reduced to avoid tip vortex cavitation. Normally the pitch distribution is closer to a constant value, as is the case with propeller V. Laminar separation of the boundary layer starts near the tip then and the separated region grows towards the hub with increasing loading, as is illustrated in Plate 3.20 (where at the higher Reynolds number also a turbulent streak is present). The laminar boundary layer region is abruptly cut off near the tip due to the occurrence of a laminar separation bubble near the leading edge. In Plate 3.20 the separation bubble is very small and therefore cannot be seen on the picture.

From the foregoing the characteristics of the boundary layer on the suction side of a propeller blade can be sketched as in Figure 8. In the region AB a laminar separation bubble occurs. The length AB is independent of the Reynolds number and depends strongly on the pressure distribution and thus on the propeller loading.

The region CD is a transition region. Its location depends on the Reynolds number, but this dependence is only weak.

The region DE is a region of laminar separation in the midchord region, which may occur near the hub. This phenomenon is independent of

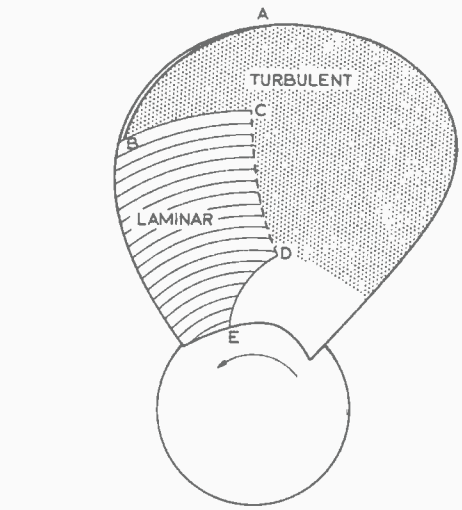


*Fig. 8. Boundary layer regions on the suction side of a propeller.*

the Reynolds number (until a critical Reynolds number, which normally exceeds the numbers used in model testing).

The cavitation behaviour of the propeller models can now be investigated and correlated with the propeller boundary layer.

# 4. Bubble cavitation

The occurrence of bubble cavitation depends on the nuclei content of the water, because every bubble cavity stems from a gas nucleus in the flow. This nucleus becomes unstable, as illustrated in Figure 1, and grows to a visible cavity. When the number of nuclei is varied this affects bubble cavitation. An example is shown in Plate 6.5, where the number of bubbles is varied by electrolysis.

When electrolysis is used small bubbles are generated on the poles: oxygen bubbles on the anode wire, hydrogen bubbles on the cathode wire. These bubbles can act as nuclei. The bubbles, produced by thin wires in a flow due to electrolysis are very small. An example is given in Plate 5.4. There the cathode wire is shown. It has a diameter of 0.9 mm. Only at higher currents the many very small bubbles, shed from the wire, coalesce in the vortices behind the wire and then they become somewhat larger in size. Since for cavitation inception near the vapor pressure a minimum bubble size is required, the current used for electrolysis should exceed a certain minimum. This gives problems at higher speeds and pressures, e.g. in a cavitation tunnel, because excessive currents are required then. Electrolysis therefore is a proper means for generating bubbles in the Depressurized Towing Tank, but is less suited for the cavitation tunnel. There application of roughness may be a substitute, as will be discussed hereafter.

In the Depressurized Towing Tank electrolysis is necessary to investigate bubble cavitation because the nuclei content of the standing water is very low. It is generally assumed that in a cavitation tunnel enough nuclei are present for proper scaling of bubble cavitation. This, however, proved to be overoptimistic, as is shown in Plate 6.6.

In the condition of Plate 6.6 application of electrolysis in the cavitation tunnel increased the amount of bubble cavitation, although

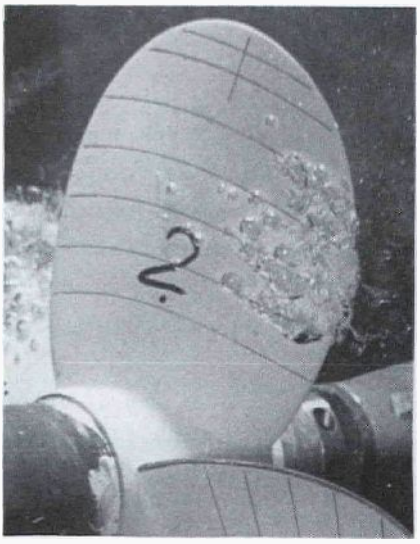

*Fig. 9. Cavitation observation in the Depressurized Towing Tank.*
*Propeller B at J=0.6 ($\sigma_n$=0.92, $Re_n$=1.1x10$^6$).*
*Smooth with electrolysis.*

only few nuclei could be generated by electrolysis because of limitations in the electrolysis current. A further increase of the nuclei content would also increase the amount of bubble cavitation further, as is shown in Figure 9. This observation was taken in the Depressurized Towing Tank, where more nuclei could be generated with electrolysis due to the lower pressure and velocity in that facility.

A cavitation pattern similar as in Figure 9 could only be obtained in the Cavitation Tunnel by drastically increasing the total air content. The test section, however, became very misty in that case and visibility was impaired.

Bubble cavitation is not influenced by the state of the boundary layer. Application of roughness at the leading edge therefore has no direct effect on bubble cavitation, as is shown e.g. in Plate 6.6.

However, the presence of a roughness element in more unfavourable conditions than in Plate 6.6 can have a strong effect. Under certain conditions such a roughness element generates nuclei from the water and thus acts as a nuclei generator.

When a single roughness element generates a stream of nuclei a bubbly spot cavity occurs, as is present in Plate 6.6. It should be noted that the roughness element or surface irregularity creating the spot can be far upstream of the beginning of the spot. Such a bubble spot consists of a number of bubble cavities, which coalesce during expansion. This type of cavitation indicates the presence of bubble cavitation on the prototype and a lack of nuclei in the water during the model test. An increase of the propeller Reynolds number makes the boundary thinner and more susceptible to surface irregularities. This is illustrated in Plate 6.12. On the smooth blade the relation between the small cavities at the leading edge and the bubble cavitation is clearly visible. In this case the nuclei are generated on many places along the leading edge and the bubbly spot cavity changes onto a fine grid of bubble cavitation. A lack of nuclei in the flow is also indicated by very large single bubble cavities, as shown in Plate 6.10 (smooth without electrolysis). In such a case the growth of a single bubble cavity is not limited by neighbouring bubble cavities and the cavity reaches a large maximum size.

Application of roughness at the leading edge can create many nuclei locally on the blade surface, which is exactly what is required, because then visibility in the test section remains unimpaired. Also the application of electrolysis is no longer necessary in that case. This can be very advantageous in case of noise measurements, because of the noise generated by the electrolysis wires themselves. The effect of leading edge roughness is shown in Plate 6.12, especially on the "smooth" propeller. Although the propeller is not artificially roughnened the surface is irregular enough to become effectively "roughened" at high Reynolds numbers. Artificial roughening of the leading edge can create this effect at a lower Reynolds number.

The question remains, of course, how many nuclei are present in the conditions on full scale ? There are indications that in sea water many small nuclei are always present, either due to breaking surfave waves or due to organic life. The number density of the nuclei on model scale should be larger than in the prototype conditions with a factor $\lambda^3$, where $\lambda$ is the scale factor. This leads to the expectation that the fine grid of bubble cavitation, as e.g. present in Plate 6.12, is closer to full scale conditions than the cavity pattern with fewer bubbles of larger size.

# 5. Sheet cavitation

Sheet cavitation proves to be very sensitive to the state of the boundary layer. As was found with the paint tests it requires very high Reynolds numbers to bring the transition region close to the leading edge, where the minimum pressure region is in case of sheet cavitation. There is, however, another mechanism which can make the boundary layer turbulent: a laminar separation bubble, as shown in Plate 3.15.

Laminar separation removes a threshold for cavitation inception, probably due to very low pressures occurring in the reattachment region at the end of the separated region. This is in contrast with inception in regions with laminar boundary layer flow, where it proves to be extremely different to create sheet cavitation, even when nuclei are abundantly present. It seems that these nuclei do not reach the low pressure region because they are pressed away by the pressure gradient near the leading edge. The larger the nuclei are, the more they are susceptible to this effect, which therefore is called "bubble screening".

The effect of a laminar boundary layer on cavitation can be seen from Plate 7.10. In that condition it was found from the paint test (Plate 3.14) that the boundary layer remained laminar near the leading edge. As a result no sheet cavitation is present, although many nuclei are available in the flow. Application of roughness at the leading edge removes the threshold for cavitation inception and a sheet cavity is formed. From Plate 7.5 it can be seen that in regions with a laminar separation bubble a sheet cavity exists. There are, however, still some regions with laminar boundary layer flow and in those regions the sheet cavity disappears and only some spots are present. These spots can be caused either by local separation or by roughness elements. The occurrence of spots is typical for a region of laminar flow where sheet cavitation is inhibited. The number of spots generally increases with increasing Reynolds number.

The existence of a laminar boundary layer suppresses sheet cavitation up to very severe conditions, as is illustrated in Plate 6.10 on the smooth blade. Some large spots at the leading edge, caused by local surface irregularities, are present, indicating that the pressure on the blades is far below the vapor pressure. Still no cavitation is present in regions with laminar boundary layer flow.

Once cavitation inception has taken place due to roughness at the leading edge the roughness should not influence the cavity shape. This indeed is not the case, see e.g. Plates 7.5 and 7.6. If this is also true very close to inception remains to be investigated. Whenever a laminar boundary layer exists on a model propeller application of roughness at the leading edge may be a proper means to prevent large scale effects.

# 6. Vortex cavitation

Inception of vortex cavitation is very sensitive to both the nuclei content and to the propeller Reynolds number. A rough indication of the inception index $\sigma_{ni}$ of tip vortex cavitation was found from a reanalysis of the literature (McCormick, 1962, Chandrashekhara, 1976) to be

$$\sigma_{ni} = 0.12\ (P/D-J)^{1.4}_{0.9R}\ Re_n^{0.35} \qquad (8)$$

Here it is assumed that sufficient nuclei are present.
An example of suppression of tip vortex inception due to a lack of nuclei is given in Figure 10.

Also the boundary layer on the blade tips can significantly change inception of the tip vortex. When the boundary layer is laminar near the blade tip, inception is detached and occurs downstream in the flow, as shown in Figure 11.

The visual determination of inception is difficult. Cavitation inception takes place incidentally somewhere along the tip vortex. Therefore another approach was developed, at least for the case of steady tip vortex cavitation, by measuring the radius $a_c$ of the cavitating tip vortex as a function of the pressure. This results in diagrams as given in Figure 12.

Two important features were found from measurements as in Figure 12. The radius of the cavitating core proved to be independent of the Reynolds number and of the total air content. This makes it possible to define an inception radius both on model scale and on the prototype, and to scale the results from the propeller model directly to the prototype.

From theoretical considerations it was found that the relation between the cavitation number and the radius of the cavitating core of the tip vortex could be written as

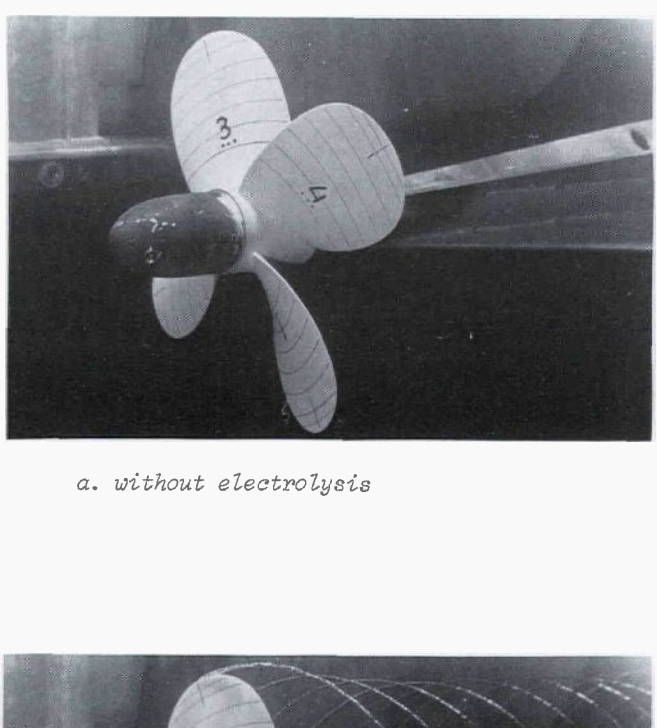

*a. without electrolysis*

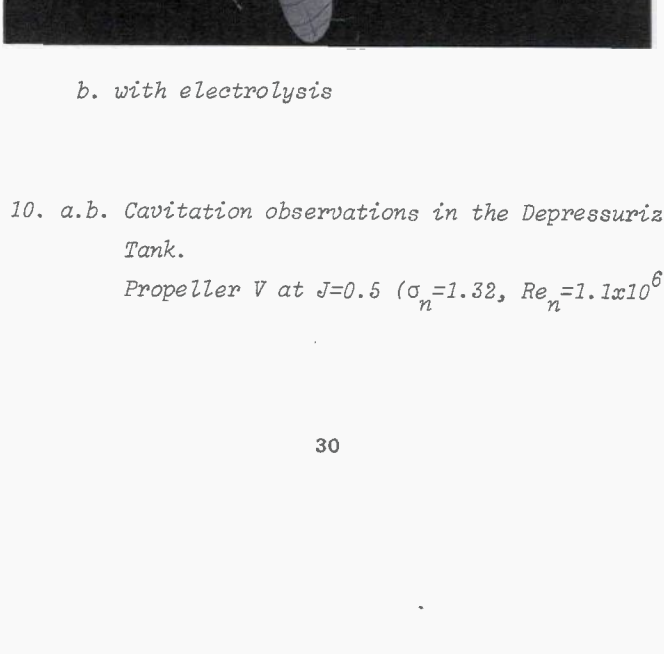

*b. with electrolysis*

*Fig. 10. a.b. Cavitation observations in the Depressurized Towing Tank.*
*Propeller V at J=0.5 ($\sigma_n$=1.32, $Re_n$=1.1x10$^6$)*

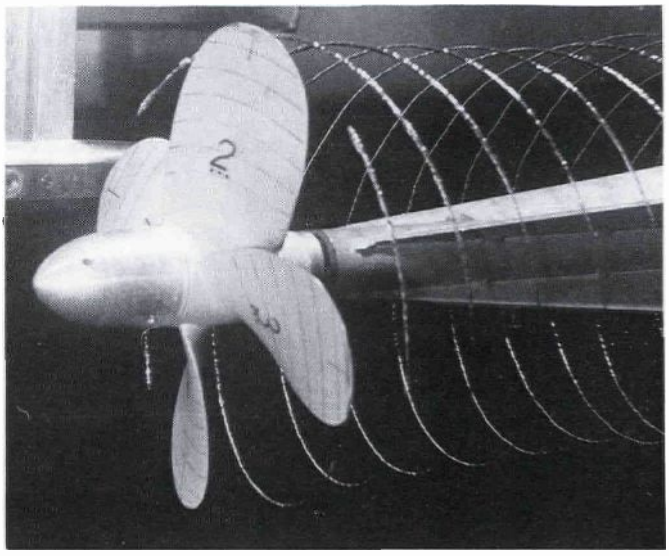

*Fig. 11. Detached cavitation inception in the Depressurized Towing Tank.*
*Propeller V at J=0.5, $Re_n$=1.1x10$^6$.*

$$\sigma = \frac{C}{a'^p_c} \qquad (9).$$

where $a'_c$ is the dimensionless cavitating core radius $a_c/D$. Both constants C and p can be found from experiments. The exponent p was found to be close to 0.25 in all cases.

The inception index on the prototype can now be found from model tests when both on the prototype and on the model a minimum radius $a_{ci}$ is defined. Then from eq. (9) it is found that

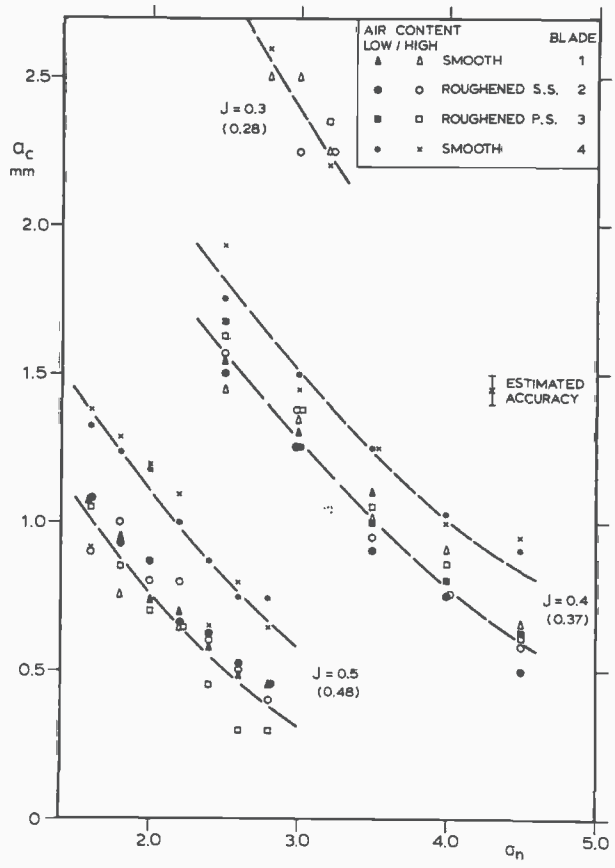


*Fig. 12. Measured radii on the cavitating core of propeller V ($Re_n$=2.76x10$^6$).*

$$\sigma_{i\ model} = \frac{C}{a'^{0.25}_{ci}} \tag{10}$$

and

$$\sigma_i(prot) = \left\{\frac{(a'_{ci})_{model}}{(a'_{ci})_{prot}}\right\}^{0.25} \sigma_i(model) \tag{11}$$

The most important asset of the approach of eq. (10) is that the inception index is derived from the cavitating conditions. This circumvents the very difficult determination of inception.

In a depressurized towing tank the Reynolds number has to be scaled with $\lambda^{3/2}$. From eq. (8) this means that $\sigma_i$ is proportional with $\lambda^{0.53}$. It is interesting to note that when the inception radii of the tip vortex are taken equal on model and full scale it follows from eq. (9) that $\sigma_i$ scales with $\lambda^{0.5}$ when p=0.25. So both approaches are compatible, although the explanation is entirely different.

An important point in the analysis, which leads to eq. (9) is that the circulation around the cavitating vortex core is not the total circulation of the tip vortex, as is often assumed, but only a small fraction of it. The tip vortex is considered as a rolled up vortex sheet outside the cavitating core.

# 7. Conclusions

1. The assumption that above a certain minimum Reynolds number laminar boundary layer flow is absent on propeller blades is not justified. This means that laminar flow effects on cavitation inception can be present on model propellers at all conditions in normal operation.

2. Sheet cavitation is strongly delayed, if not totally inhibited, by the presence of a laminar boundary layer in the low pressure region on the blades.

3. Laminar separation occurs frequently on model propellers. The presence of a laminar separation bubble removes the threshold for cavitation inception. On model scale sheet cavitation will therefore occur in regions with laminar separation only.

4. When the Reynolds number is increased the laminar boundary layer becomes more sensitive to surface irregularities or to particles attached to the propeller blades. These disturbances may cause turbulent streaks in the boundary layer, which in cavitating condition result in spot cavities from the leading edge. The presence of spot cavities is an indication that laminar boundary layer flow inhibits sheet cavitation.

5. The radial extent of a laminar separation bubble is strongly dependent on manufacturing accuracy of the blades and on blade loading. This may overemphasise the sensitivity of sheet cavitation to the propeller loading and may cause differences in cavitation behaviour between blades on the model propeller.

6. Application of roughness at the leading edge can be a method to stimulate cavitation inception in regions with a laminar boundary layer, thereby improving the correlation between model and prototype.

7. Bubble cavitation is insentitive to the propeller boundary layer. An increase of the propeller Reynolds number increases the test section pressure, which may decrease the number of nuclei. The effect is a decrease of bubble cavitation.

8. An increase of the propeller Reynolds number increases the effect of surface irregularities. In case of bubble cavitation the effect is that surface irregularities may generate nuclei from the flow. These nuclei cause a bubbly spot cavity when the cavitation number is low enough. These spot cavities, which start away from the leading edge, are an indication of a lack of nuclei.

9. When only very few nuclei are present in the flow large isolated bubble cavities are formed in regions with a low pressure. These large cavities are also indications of a lack of nuclei.

10. Application of roughness at the leading edge may be a proper means to generate an abundant amount of nuclei locally on the blades. This leads to a fine grid of small bubble cavities, which probably better simulates the cavitation on the prototype.

11. Electrolysis may also be a method to generate additional nuclei. This method is most suited for low pressures and low speeds. In the Depressurized Towing Tank electrolysis therefore is a useful tool. In a cavitation tunnel other methods may be better. Both facilities require artificial supply of nuclei for proper simulation of the prototype conditions.

12. There are two ways of scaling tip vortex inception. The usual way is by viscous effects. An alternative approach is inviscid, where the total circulation of the vortex is not concentrated around the cavitating core. Both approaches lead to similar results. The advantage of the inviscid approach is that the very difficult cavitation inception measurements are avoided.

NOMENCLATURE

| | | Dimension |
|---|---|---|
| $a_c$ | radius of the cavitating vortex core | m |
| $C_p$ | pressure coefficient $\frac{p-p_o}{\frac{1}{2}\rho V^2}$ | - |
| c | chord length of a propeller section | m |
| D | propeller diameter | m |
| J | advance ratio $\frac{U}{nD}$ | - |
| K | constant representing the amount of gas in a bubble | Nm |
| n | number of propeller revolutions | $sec^{-1}$ |
| $p_o$ | pressure in the fluid | - |
| $p_v$ | vapor pressure | $Nm^{-2}$ |
| $R_{crit}$ | critical bubble radius | m |
| Re | sectional Reynolds number $\frac{V.c}{\nu}$ | - |
| $Re_n$ | propeller Reynolds number $\frac{nD^2}{\nu}$ | - |
| s | surface tension | $Nm^{-1}$ |
| U | axial velocity of propeller | $m\ sec^{-1}$ |
| V | undisturbed inflow velocity of a propeller section | $m\ sec^{-1}$ |
| $\lambda$ | scale ratio | - |
| $\nu$ | kinematic viscosity of fluid | $m^2 sec^{-1}$ |
| $\rho$ | specific mass of fluid | $kg\ m^{-3}$ |
| $\sigma$ | sectional cavitation index $\frac{p_o-p_v}{\frac{1}{2}\rho V^2}$ | - |
| $\sigma_n$ | propeller cavitation index $\frac{p_o-p_v}{\frac{1}{2}\rho n^2 D^2}$ | |

APPENDIX

In this appendix some short comments on the Plates will be given:

Plate 3.1. : The smooth blade illustrates that a laminar boundary layer exists, even at this high Reynolds number. The roughened blade shows that application of roughness was effective in removing the laminar regions.

Plate 3.4. : Illustrates that the paint test reproduce on propellers of different size at the same Reynolds number.

Plate 3.10.: The increase of Reynolds number moves the transition region towards the leading edge. However, in regions with a favourable pressure gradient the boundary layer remains laminar. The minimum pressure is in the midchord region.

Plate 3.11.: Also when a low pressure peak exists at the leading edge the boundary layer remains laminar until the pressure gradient becomes adverse.

Plate 3.14.: In this case the pressure distribution is similar as in Plate 3.11, but the minimum pressure occurs closer to the leading edge because of the thinner blade sections. The boundary layer behind the minimum pressure peak is thinner than in Plate 3.11 and therefore more sensitive to surface irregularities. At $Re_n=1.7x10^6$ turbulent streaks disturb the laminar boundary layer region, which will lead to spot cavities.

Plate 3.15.: Illustrates the occurrence of a laminar separation bubble. The differences between both blades illustrate the sensitivity of laminar separation to the blade geometry. This leads to differences in the radial extent of sheet cavitation.
On Blade 2 some indications of a laminar boundary layer are present around r/R=0.8. In this region a gap was always found in the sheet cavity on this blade.

Plate 3.17.: Differences between the blade geometry, especially at the leading edge, are emphasized by laminar separation. This plate shows these differences, which in cavitating conditions will lead to differences in sheet cavitation between the blades.

Plate 3.18.: Shows how the separated region varied with the blade loading. In cavitating conditions the sheet cavity would be restricted to the region of separated flow.

Plate 3.13.: The advance ratio is misprinted as J=0.28 instead of 0.85. At this very high propeller loading still no laminar separation occurs over much of the radius because the blade sections of propeller B are thicker than usual. A separated region seems present outside r=0.8. This shows the strong influence of the blade section profiles on the boundary layer behaviour.

Plate 3.12.: The advance ratio here is J=0.85. At this very light loading the propeller boundary layer becomes fully laminar with a tendency to separate near the trailing edge. This despite the fact that the Reynolds number is still generally assumed to be sufficient to avoid laminar flow effects.

Plate 3.20.: The loading at the tip of this propeller is heavier than on propellers S and B. This is reflected by the laminar separation region, which occurs near the tip flow. Note the difference between both blades and the turbulent streak on blade 2.

Plate 5.4. : The generation of hydrogen bubbles from a wire was observed for various currents. At I=16.0 A/m larger bubbles are forced in the Karmán vortices behind the wire. These bubbles are of the order of 0.2 mm in diameter.

Plate 6.5. : The amount of bubble cavitation depends on the nuclei generated by electrolysis. Note that at 0.4 A/m cavities are large, becoming smaller when more nuclei are present.

Plate 6.6. : The minimum pressure in this condition is in the midchord region. The bubbly spot cavity at r/R=0.75 is caused by some roughness element at this radius. On blade 1 it is visible that nuclei expand before forming the spot cavity. Note the rather large bubble cavities on the blades with electrolysis, indicating that the amount of nuclei was still small.

Plate 6.10.: The minimum pressure is near the leading edge in this case. Sheet and bubble cavitation merge. Note that when the boundary layer at the leading edge remains laminar and attached, no sheet cavitation is present, even at this high Reynolds

number. Note also the very large bubble cavity on blade 4 without electrolysis. On the roughened blade at inner radii the roughness elements generate enough nuclei to cause bubble cavitation in the midchord region.

Plate 6.12.: This is the highest Reynolds number which could be obtained in the cavitation tunnel. The propeller is propeller B. The smooth blade exhibits small cavitation streaks at the leading edge which supply the nuclei for the bubble cavitation on midchord. Application of roughness causes the leading edge sheet to develop and the cavitation picture changes drastically.

Plate 7.10.: Although many bubbles are present in the flow the sheet is not formed on the smooth blade because the boundary layer remains laminar (Plate 3.14). Roughness does create a sheet cavity at radii where the minimum pressure is below the vapour pressure.

Plate 7.5. : Note the three-dimensional structure of the sheet cavity. At inner radii small cavitating vortex cores seem to occur on top of the sheet. When the cavity length increases with the radius the end of the cavity is remarkably stable. When this is not so a strong entrainment occurs. The gap in the sheet of the smooth blade is exactly where laminar boundary layer flow was sometimes observed in the paint tests.

Plate 7.6. : At a higher pressure the phenomena remain similar as in the previous picture, plate 7.5.